Regular and Singular Behaviours and New Morphologies in the Rayleigh Taylor Instability

Kurt Williams, Desmond L. Hill, Snezhana I. Abarzhi

Abstract The Rayleigh Taylor Instability is a fluid instability that develops when fluids of different densities are accelerated against their density gradient. Its applications include inertial confinement fusion, supernovae explosion, fossil fuel extraction and nano fabrication. We study Rayleigh Taylor instability developing at an interface with a spatially periodic perturbation under a time varying acceleration using group theoretic methods. For the first time, to our knowledge, both regular and singular nonlinear solutions are found, which correspond to the structure of bubbles and spikes emerging at the interface. We find that the dynamics of bubbles is regular, and the dynamics of spikes is singular in an asymptotic time-regime. The parameters affecting the behaviour of both bubble and spikes are discussed, including the inter-facial shear, which is shown to have a profound effect. The results set key theoretical benchmarks for future analysis.

1 Introduction

1.1 Rayleigh Taylor Instability

The problem of Rayleigh Taylor instability was first systematically studied in 1883[12] by Lord Rayleigh, who proposed an experiment in which a dense fluid (eg: water) is balanced on top of a less dense fluid (eg: oil). The system, if perfectly balanced, would remain at rest - with the dense fluid on top being unable to penetrate the lighter fluid. However, any perturbation or deviation away from this equilibrium state causes the system to rapidly accelerate away from the equilibrium state. Later experiments by Taylor [7] would confirm the unstable nature of such a system and

Snezhana I. Abarzhi
School of Mathematics and Statistics, The University of Western Australia
e-mail: snezhana.abarzhi@gmail.com

provide geometric insight about the problem.

In the most general of terms, the Rayleigh Taylor Instability can be defined to be a system of two fluids of different densities undergoing a prolonged acceleration normal to the interface between the fluids. In a system with this configuration, the less dense fluid "bubbles" up and penetrates the denser fluid, which itself penetrates the lighter fluid as "spikes". Both "bubble" and "spike" structures are observed to have a finger-like structure that is paraboloidal in nature for early time, but may evolve into more irregular structures in the late-time 'mixing' regime.

In a complete description of the system, shearing forces that emerge at the interface are responsible for deformations of these bubble and spike structures. Whilst at very small scales, this vortical behaviour can be described independently, as has been done in research of Kelvin Helmholtz instabilities, for the Rayleigh Taylor instability, these structures are tiny, and shear is best described as a global property of the system that can affect its growth and other behaviour.

Rayleigh Taylor behaviours are observed in a broad range of circumstances and scales. Examples in nature include supernovae[4], galactic evolution [4], and ocean dynamics [1]. Industrial examples include laser micromachining [13] (including laser ablation [5]), inertial confinement fusion [9], optical telecommunications [11] and aeronautics [6]. With such a large range of fundamental processes being driven by Rayleigh Taylor dynamics, it is vital that effective theoretical benchmarks are set.

2 Theoretical Approach

2.1 Governing Equations

2.1.1 Euler Lagrange Equations

The analytic description of the system begins with the Euler equations for incompressible fluids of uniform density:

$$\frac{D\mathbf{u}}{Dt} = -\nabla\omega + \mathbf{g} \tag{1}$$

$$\nabla \cdot \mathbf{u} = 0 \tag{2}$$

By considering an infinitesimal volume dV of fluid, the conservation of mass, momentum and energy lead to the following conservation equations:

$$\frac{\partial}{\partial x_i}(\rho v_i) = \frac{\partial \rho}{\partial t} \tag{3}$$

$$\frac{\partial \rho v_i}{\partial t} + \sum_{j=1}^{3} \frac{\partial \rho v_i v_j}{\partial x_i} + \frac{\partial P}{\partial x_i} = 0 \tag{4}$$

$$\frac{\partial E}{\partial t} + \frac{\partial (E+P) v_i}{\partial x_i} = 0 \tag{5}$$

where in these equations, ρ is the density, p is the momentum, v_i are the components of the velocity field, x_i are the spatial coordinates of the system and E and P are the energy and pressure respectively. The energy can also be expressed as $E = \rho(e + \mathbf{v}^2/2)$ for specific internal energy e.

2.2 Interface Conditions

In order to separate the dynamics of both the bulk and the interface, we introduce a scalar function $\theta(\rho, \mathbf{v}, P, E)$ which has derivatives of at least first order (i.e. $\nabla\theta$ and $\dot{\theta}$ exist), with θ being 0 at the interface of the two fluids. Then the denser fluid is located in the region $\theta > 0$ and the less dense fluid fills the region $\theta < 0$.

Since these two fluids are perfectly separated by this boundary of $\theta = 0$, we may express our total domain as $(\rho, \mathbf{v}, P, E) = (\rho, \mathbf{v}, P, E)_h H(\theta) + (\rho, \mathbf{v}, P, E)_l H(-\theta)$. Substituting into the conservation equations, we obtain the following conditions at the interface:

$$\begin{aligned} [\mathbf{j} \cdot \mathbf{n}] &= 0 & [(P + \frac{(\mathbf{j} \cdot n)^2}{\rho})\mathbf{n}] &= 0 \\ [(\mathbf{j} \cdot \mathbf{n})(\frac{(\mathbf{j} \cdot \tau)}{\rho})\tau] &= 0 & [(\mathbf{j} \cdot \mathbf{n})(W + \frac{(\mathbf{j})^2}{2\rho^2})] &= 0 \\ \mathbf{n} &= \frac{\nabla\theta}{|\nabla\theta|} & \mathbf{n} \cdot \tau &= 0 \end{aligned} \tag{6}$$

where the square brackets [...] denote the "jump" of the function across the interface - essentially the limit of the derivative with respect to θ. The mass flux is expressed as $\mathbf{j}$.

In the case in which there is no mass flux across the interface ($\mathbf{j} \cdot \mathbf{n}|_{\theta=0^{\pm}} = 0$), these boundary conditions at the interface become:

$$[\mathbf{v} \cdot \mathbf{n}] = 0, [P] = 0, [\mathbf{v} \cdot \tau] = arbitrary, [W] = arbitrary \tag{7}$$

and at infinity:

$$\lim_{z\to\infty} v_h = 0, \lim_{z\to-\infty} v_l = 0 \tag{8}$$

Whilst there exist two natural time scales for Rayleigh Taylor systems with time-varying acceleration [10], we will focus on the the timescale of acceleration-driven dynamics. The two timescales are $\tau_g = (kG)^{-1/(a+2)}$ and $\tau_0 = 1/(k|v_0|)$ with $|v_0|$ some initial growth rate for the system. Furthermore, there is a unique length scale $1/k$ imposed by the wave vector.

2.3 Large Scale Dynamics

Any vector field can be expressed as the sum of the gradient a scalar potential plus the curl of a vector potential field. In this way, we may express our vector field as:

$$\mathbf{v} = \nabla\Phi + \nabla\times\phi \tag{9}$$

The large scale dynamics are assumed to be irrotational, since no discontinuities or circulations occur. The small-scale dynamics are rotational, but by Kelvin's Circulation Theorem the large scale dynamics are irrotational in the bulk [14]. We hence set $\nabla\times\phi = 0$. This means that the velocity field $\mathbf{v}$ can be expressed as $\nabla\Phi$.

By substituting this expression for $\mathbf{v}$ into the conservation equations, we obtain the following:

$$\Delta\Phi = 0 \tag{10}$$

$$\rho(\frac{\partial\Phi}{\partial t} + \frac{\nabla\Phi^2}{2}) + P = 0 \tag{11}$$

Now substituting the expression for $\mathbf{v}$ into 7, we obtain a system of equations to solve:

$$\rho_h(\nabla\Phi_h\cdot\mathbf{n} + \frac{\dot\theta}{|\nabla\theta|}) = \rho_l(\nabla\Phi_l\cdot\mathbf{n} + \frac{\dot\theta}{|\nabla\theta|}) = 0 \tag{12}$$

$$\nabla\Phi_h\cdot\tau - \nabla\Phi_l\cdot\tau = arbitrary \tag{13}$$

$$\rho_h(\frac{\partial\Phi_h}{\partial t} + \frac{|\nabla\Phi_h|^2}{2} + (g(t) + \frac{\partial v}{\partial z})z) = \rho_l(\frac{\partial\Phi_l}{\partial t} + \frac{|\nabla\Phi_l|^2}{2} + (g(t) + \frac{\partial v}{\partial z})z) \tag{14}$$

where $g(t) = Gt^a$, a power-law function of time. In the frame of reference that moves with the bubble tip, the boundary conditions are instead expressed:

$$\nabla\Phi_h|_{z\to\infty} = (0,0,-v(t)), \nabla\Phi_l|_{z\to-\infty} = (0,0,-v(t)), \tag{15}$$

2.4 Group Theory

In order to capture the highly-symmetric nature of our solution, we appeal to group theory. The interface between the two fluids is initially flat, or rather very close to flat and so is essentially $\mathbb{R}^2$, a group of Lie Type, which is to say that $\mathbb{R}^2$ under some set of transformations, can be considered to be both a group and a manifold. The elements of the irreducible representations of this group will inform the structure of Fourier series over the group. Since we are seeking a solution which has symmetries over the entire space, we infer that the group operations in question must be symmetry transforms on $\mathbb{R}^2$. There are seventeen groups of invariants under these transformations, but by imposing the condition that our structures must have inversions along the interfacial plane, and must be repeating, we need only consider the two-dimensional groups p2mm, p4mm, p6mm, p2 and cmm for three dimensional flows; and the one-dimensional group p1m for two-dimensional flows. These groups are referred to using the international notation [2]. In this notation, *m*'s denote the number of reflective or "mirroring" symmetries a cell has, *p*'s indicate primitive cells - which have natural translational symmetries, *c*'s denote face-centred cells and free numbers indicate the rotational symmetry of each cell.

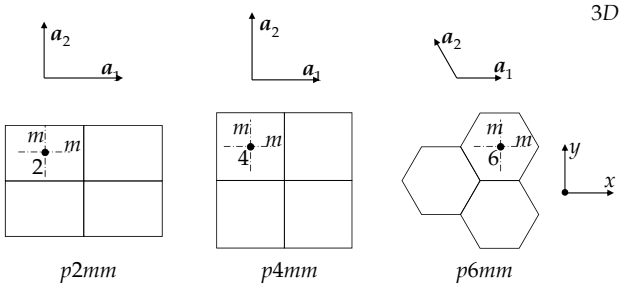

Fig. 1 A selection of the seventeen unique wallpaper groups.

We will be examining the symmetry group p6mm, which has six rotational symmetries, 2 reflective symmetries and three directions of equal magnitude translational symmetry, the third of these being the direct sum of the first two. The naive treatment of such a structure would be to construct vectors $\mathbf{a}_i$ along each edge and express our solution in terms of these. However, to actually express our solution, we need to map these "lattice vectors" into reciprocal space - a non-euclidean manifold in which the metric for distances between two points is:

$$d(x,y) = 1/d_E(x,y), \tag{16}$$

where d_E is the Euclidean metric. Each of the vectors $\mathbf{k}_j$ in inverse space obeys the relationship $\mathbf{a}_i \cdot \mathbf{k}_j = 2\pi$, for $i, j \in 1,2$ and $\mathbf{k}_3 = \mathbf{k}_1 + \mathbf{k}_2$. Since the lattice vec-

tors are $(2\pi)\mathbf{a}_i = \{(1,0),(-0.5,\sqrt{3}/2),(-0.5,-\sqrt{3}/2)\}$, our reciprocal vectors are $(\sqrt{3}\lambda/4\pi)\mathbf{k}_j = \{(\sqrt{3}/2,1/2),(0,1),$
$(\sqrt{3}/2,-1/2)\}$. There is an interesting geometric relation between the lattice vectors and the reciprocal lattice vectors in euclidean space - the reciprocal vectors form a basis for the centre of each cell (figure 2). As such, these vectors are the basis for a Fourier series of structures along the interface.

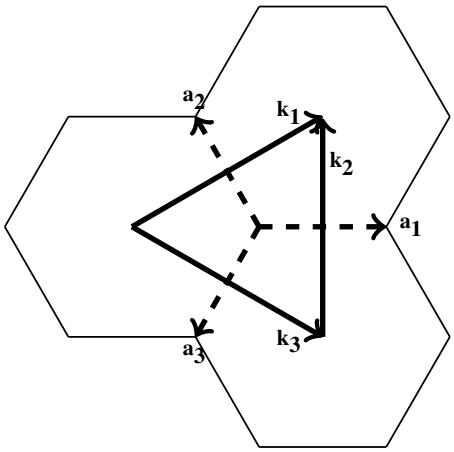

Fig. 2 The geometric relationship between the lattice vectors $\mathbf{a}_i$ (dashed) and the reciprocal vectors $\mathbf{k}_j$ (solid)

So then, since we require the maxima of our Fourier series along the interface to be at the centre of the hexagonal cells, we expect our Fourier series for the velocity potential to be of the form:

$$\Phi \sim \sum_{j=1}^{3} \cos(\alpha \mathbf{k}_j \cdot \mathbf{r})$$

Then summing over all the modes of harmonics and the boundary conditions for the heavy and light fluids, we obtain in a single step:

$$\Phi_h(\mathbf{r},z,t) = \sum_{m=0}^{\infty} \Phi_m(t)(z + e^{\frac{-mkz}{3mk}} \sum_{j=1}^{3} \cos(m\mathbf{k}_j \cdot \mathbf{r})) + f_h \tag{17}$$

$$\Phi_l(\mathbf{r},z,t) = \sum_{m=0}^{\infty} \hat{\Phi}_m(t)(-z + e^{\frac{mkz}{3mk}} \sum_{j=1}^{3} \cos(m\mathbf{k}_j \cdot \mathbf{r})) + f_l \tag{18}$$

where $\mathbf{r} = (x,y)$ is the position along the interface, Φ_m and $\hat{\Phi}_m$ are the Fourier amplitudes, with $m \in \mathbb{Z}$. It is worth noting that $|\mathbf{a}_i| = \lambda$, $k = |\mathbf{k}_i| = 4\pi/(\lambda\sqrt{3})$.

We are interested in the motion at the tips of the bubbles and spikes, so we are able to Taylor expand the scalar function $\theta(z) = z - z^*(x,y,t)$. Knowing that the structures are symmetric about the centre of each "symmetry cell", the expansion is:

$$z^*(x,y,t) = \sum_{N=1}^{\infty} \zeta_N(t)\mathbf{r}^{2N}. \tag{19}$$

To the first order (N=1), the tip expansion is $z^* = \zeta(x^2+y^2)$.

2.5 The Moments Expansion

Since the equation is expanded in terms of harmonics of standing waves (17), it would be natural to truncate the series to a few terms and analyse those. However, much of the behaviour of the system is governed by the interplay between these harmonics. In order to preserve these harmonics in our equations we introduce weighted sums over all the harmonics known as "moments":

$$M_n = \sum_{m=0}^{\infty} \Phi_m(t)k^n m^n \tag{20}$$

$$\hat{M}_n = \sum_{m=0}^{\infty} \hat{\Phi}_m(t)k^n m^n \tag{21}$$

2.6 The Dynamical System

Finally, having attained local expressions for the potential field and the interface, we substitute into 12-2.14 and obtain the following system of equations:

$$(1+A)(\dot{\zeta} - 2\zeta M_1 - \frac{M_2}{4}) = (1-A)(\dot{\zeta} - 2\zeta\hat{M}_1 + \frac{\hat{M}_2}{4}) = 0 \tag{22}$$

$$(1+A)(\frac{\dot{M}_1}{4} + \zeta\dot{M}_0 - \frac{M_1^2}{8} + \zeta g) = (1-A)(\frac{\dot{\hat{M}}_1}{4} + \zeta\dot{\hat{M}}_0 - \frac{\hat{M}_1^2}{8} + \zeta g) \tag{23}$$

$$M_1 - \hat{M}_1 = arbitrary, \qquad M_0 = -\hat{M}_0 = -v \tag{24}$$

Where $A = (\rho_h - \rho_l)/(\rho_h + \rho_l)$, the Atwood number and $g = g(t) = Gt^a$.

2.7 Early Time Solutions

For the early time solutions, only the first harmonics are retained in the expressions, yielding:

$$\begin{aligned} M_i &= -\hat{M}_i = -k^i v, \qquad v = \frac{4}{k^2}\dot{\zeta} \\ (1+A)(\ddot{\zeta} - \zeta G t^a) &= (1-A)(-\ddot{\zeta} - \zeta G t^a) \end{aligned} \tag{25}$$

This system of equations has general solution:

$$\zeta(t) = c_1\sqrt{\frac{t}{\tau}} I_{\frac{1}{2s}}(\sqrt{AG}\frac{(\frac{t}{\tau})^s}{s}) + c_2\sqrt{\frac{t}{\tau}} I_{-\frac{1}{2s}}(\sqrt{AG}\frac{(\frac{t}{\tau})^s}{s}) \tag{26}$$

With $\tau = \tau_g$ being the characteristic timescale of the time-dependent acceleration force. The case $a = 0$ yields the classic result:

$$\zeta(t) = c_1 \exp(\sqrt{AG}\frac{t}{\tau}) + c_2 \exp(\sqrt{AG}\frac{t}{\tau}) \tag{27}$$

2.8 Nonlinear Dynamics

In general the dynamical system is not solvable. We can, however, generate an asymptotic solution in the regime of $t \to \infty$. In such a regime, we assume that each of the modes of oscillation grow at the same rate, since otherwise our problem is dominated by a single mode which could be analysed in exactly the same way as our linear, early time dynamics. We also assume that the rate of growth goes as some power law expansion of time, which is to say that the growth of these modes is governed by the external acceleration, which has power-law dependence on time. We presume that asymptotically:

$$\zeta \sim t^a, \qquad (M, \hat{M}, \Phi, \hat{\Phi}) \sim (m, \hat{m}, \phi, \hat{\phi}) t^\beta$$

In order to ensure our solution resolves issues of closure, and captures the interaction between harmonic modes, we expand our moments to the second mode of oscillation:

$$M_n(t) = (\Phi_1(t) + 2^n \Phi_2(t))k^n, \qquad \hat{M}_n(t) = (\hat{\Phi}_1(t) + 2^n \hat{\Phi}_2(t))k^n \tag{28}$$

Which yields the following:

$$\zeta_1 = -\frac{m_2}{8m_1} \qquad \zeta_1 = -\frac{\hat{m}_2}{8\hat{m}_1} \tag{29}$$

$$m_1 = \frac{2m_0 k}{3-8p} \qquad \hat{m}_1 = \frac{2\hat{m}_0}{3+8p} \tag{30}$$

$$m_2 = 3km_1 - 2k^2 m_0 \qquad \hat{m}_2 = 3k\hat{m}_1 - 2k^2\hat{m}_0 \tag{31}$$

$$p = -\frac{\zeta}{k} \tag{32}$$

Substituting these into equation 23, we obtain:

$$\begin{aligned}(1+A)(\frac{bm_1}{4}+\zeta_1 bm_0-\frac{m_1^2}{8}t^{1+b}-\zeta_1 Gt^{1+a-b})\\ =(1-A)(\frac{b\hat{m}_1}{4}-\zeta_1 b\hat{m}_0-\frac{\hat{m}_1^2}{8}t^{1+b}-\zeta_1 Gt^{1+a-b})\end{aligned} \tag{33}$$

In determining solutions to this equation, we invoke dominant balance and find three potential balances:

$$a<-2, b=-1 \qquad a=-2, b=-1 \qquad -2<a, b=\frac{a}{2}$$

If a is sufficiently small ($a<-2$), then the external acceleration will have negligible effect, and the motion will essentially be of Richtmyer Meshkov type. The second case will be a threshold point at which the dynamics will be both of Rayleigh Taylor and Richtmyer Meshkov type. The Rayleigh Taylor dynamics are given in the third case. In letting $b=a/2$ and $-2<a<0$, we solve for the velocity:

$$v(t)=-\frac{\sqrt{G(t/\tau)^a}}{k}(64p^2-9)\sqrt{\frac{2Ap}{48p+A(64p^2+9)}} \tag{34}$$

$$=-\frac{1}{\tau k}(\frac{t}{\tau})^{a/2}(64p^2-9)\sqrt{\frac{2Ap}{48p+A(64p^2+9)}} \tag{35}$$

The structure with the fastest velocity for a given Atwood number is known as the Atwood structure. Setting the time derivative of $v(t)$ to be zero yields the following condition for the curvature ($p=p^*$) and velocity ($v(t)=v^*(t)$) of an Atwood structure:

$$\begin{aligned}p^{*4}+\frac{1}{A}p^{*3}+\frac{9}{32}p^{*2}-(\frac{3}{16})^3=0\\ \implies v^*(t)=-\frac{1}{\tau k}(\frac{t}{\tau})^{a/2}(8p^*)^{\frac{3}{2}}\end{aligned} \tag{36}$$

We also seek to account for the vortical structures that emerge strictly at the interface. Although they do not cause global circulation, they do provide a means by which the two fluids can move or "shear" past each other. We thus introduce a global parameter to quantitatively measure this interfacial shearing:

$$\Gamma(\zeta,t)=M_1(t)-\hat{M}_1(t)=\frac{12k}{64p^2-9}v(t) \tag{37}$$

In all of our equations, the curvature (ζ) and wavelength (k) are natural parameters of the system. Since the wavelength is fixed by the initial configuration of our system it is natural to assume, as Garabedian[8] did, that solutions to the problem of Rayleigh Taylor instability form a one-parameter family of solutions, and that the dynamics are single-scale in nature. So then, our full description of the system is:

$$v(t) = -\frac{1}{\tau k}\left(\frac{t}{\tau}\right)^{a/2}(64p^2-9)\sqrt{\frac{2Ap}{48p+A(64p^2+9)}}$$
$$\Gamma(\zeta,t) = \frac{12k}{64p^2-9}v(t) \tag{38}$$

3 Bubble Dynamics

Bubbles are formed when the lighter fluid penetrates into the heavy fluid. As such, they are concave downwards in z and have negative curvature ($\zeta < 0$, $p > 0$). In the asymptotic limit, the velocity function is shown in figure 3.

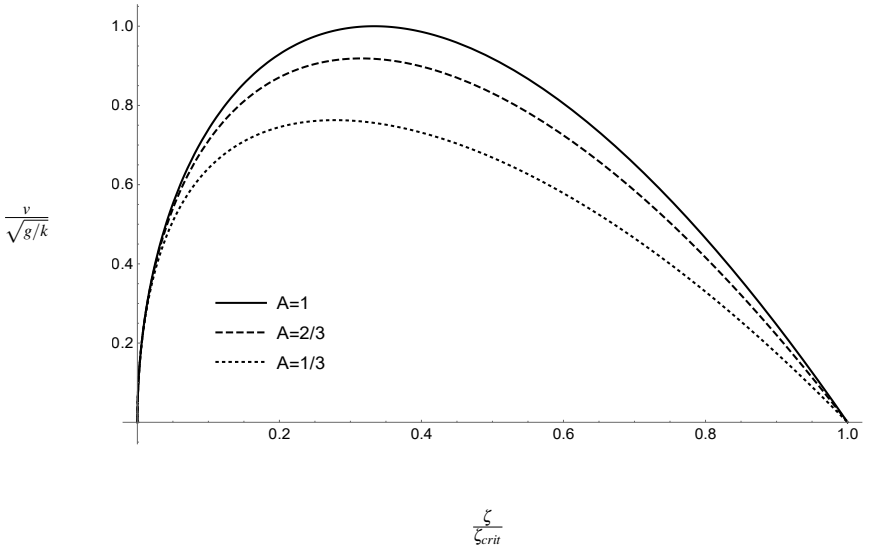

Fig. 3 The velocity (v) of a rising bubble scaled by growth rate ($\sqrt{g/k}$, $g = Gt^a$) as a function of its curvature (ζ).

We clearly observe that there is a one-parameter family of solutions. For any given Atwood number, there is a broad range of possible curvatures, each with its own velocity. The curvature of each solution is uniquely determined by the initial interface perturbation.

The behaviour seen in figure 3 makes physical sense. If the interface is perfectly flat ($\zeta = 0$), then there is no dynamic motion and the velocity is zero. However, any curvature in the interface will allow the heavy fluid to sink and the resultant bubble to rise up. Thinner bubbles grow faster, and it appears that there is a positive cor-

relation between curvature and velocity. However, at a sufficient curvature (which depends on the Atwood number), there is a maximally fast bubble, and at curvatures higher than this, the velocity becomes decreases with curvature. The velocity eventually approaches zero at the critical curvature ($\zeta = -3/8k$). This unique curvature is a stagnation point for the system.

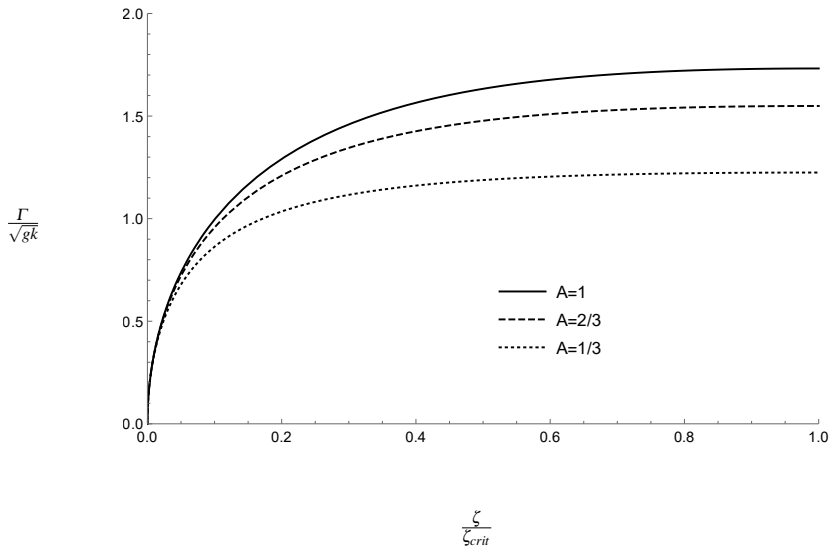

Fig. 4 The intefacial shear (Γ) scaled by growth rate ($\sqrt{gk}$, $g = Gt^a$) as a function of its curvature (ζ), note that larger Atwood numbers give a larger interfacial shear.

The interfacial shearing continuously grows with curvature (figure 4), and is maximal at $\zeta = -3/8k$. We conclude that whilst the interfacial shearing does grow with velocity, it eventually dominates the dynamics and those solutions with maximal shear do have a lower velocity. Thus, whilst the interfacial shearing is dependent on the velocity, it is a competing mechanism in the dynamics and resists rising bubbles reaching their maximal velocity. The velocity is highly sensitive to this interfacial shearing and nonlinear bubbles have a multiscale dependence on both the curvature (a parameter governing its effective acceleration) and the interfacial shear.

In any case, we expect the dynamics to be dominated by the bubble exhibiting the highest velocity, which we herein call the "Atwood" bubble. Numerical simulations involving competing bubbles of various velocities demonstrate that asymptotic dynamics are dominated by bubbles with the highest velocity [3]. We thus expect the Atwood solution to be the physically relevant one.

We can therefore conclude that there is a one-parameter family of solutions that

arises due to the multiscale character of the dynamics. The dynamics is multiscale and governed by the interaction of acceleration and the interfacial shearing. However, any system will be dominated by the fastest or "Atwood" type solution in the asymptotic regime.

4 Spike Dynamics

Spikes are the complementary structure of bubbles. They are concave in the positive θ direction and flow from the heavy fluid into the light ($v < 0$), they have positive curvature ($\zeta > 0$, $p < 0$). The asymptotic velocity has the form seen in figure 5.

There are a number of unique features in the asymptotic velocities of the spikes.

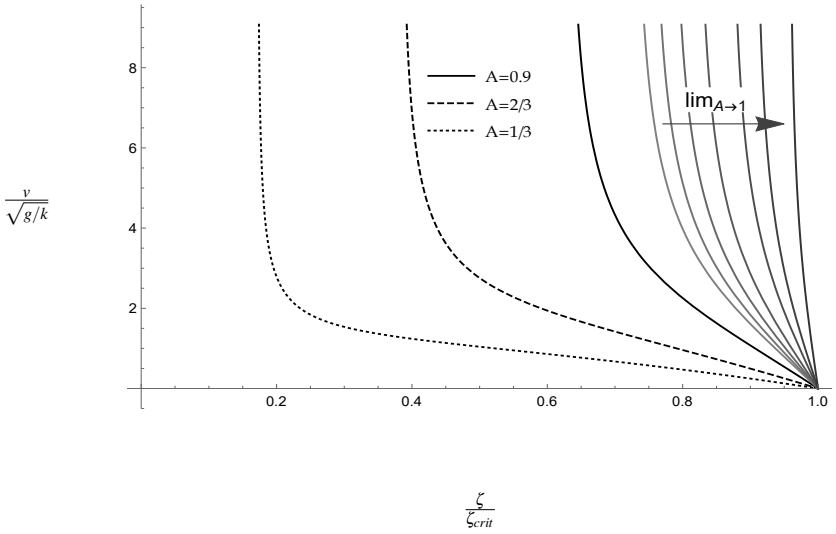

Fig. 5 The dependence of spike velocity (v) scaled by growth rate ($\sqrt{g/k}$, $g = Gt^a$) on the curvature (ζ). The dynamics as $A \to 1$ is unbounded for all curvatures less than the critical curvature.

Much like bubbles, there is a critical curvature ($\zeta = 3/8k$) which forms a stagnation point for spikes. Unlike bubbles, however, spikes with very small curvatures ($\zeta \to 0$) do not tend towards stagnation, but reach unbounded growth. It may be tempting to suggest that these singularities are nonphysical, but they correspond to unbounded growth in the asymptotic ($t \to \infty$) regime. This is not nonphysical. Furthermore, our analysis has restricted itself to finding dynamics on the order $\sim k$. A singular velocity suggests that the dynamics of the system outgrows this scale. This growth is likely the mechanism for the transition between the nonlinear dynamics and the mixing regime. Thus, this analysis could open the door to understanding the

hitherto unexplored mixing regime.

The exact scaled curvature at which the spike velocity becomes asymptotic is $\kappa(A)k$, where:

$$\kappa(A) = \frac{3}{8}\frac{1-\sqrt{1-A^2}}{A} \tag{39}$$

And it is interesting to note that at this curvature, the interfacial shearing is also singular (figure 6), suggesting that the dynamics grows beyond $\sim k$ in both of the associated scales (wavelength and amplitude). As such, the effect of interfacial shear is not dominated by this unbounded growth in velocity and the dynamics of the spikes is also to be understood as a multiscale phenomenon. It should also be noted that in the limit of the density of the lighter fluid tending towards zero ($A \to 1$), the spike velocity becomes unbounded for all curvatures less than the stagnant critical curvature ($\zeta = 3/8k$).

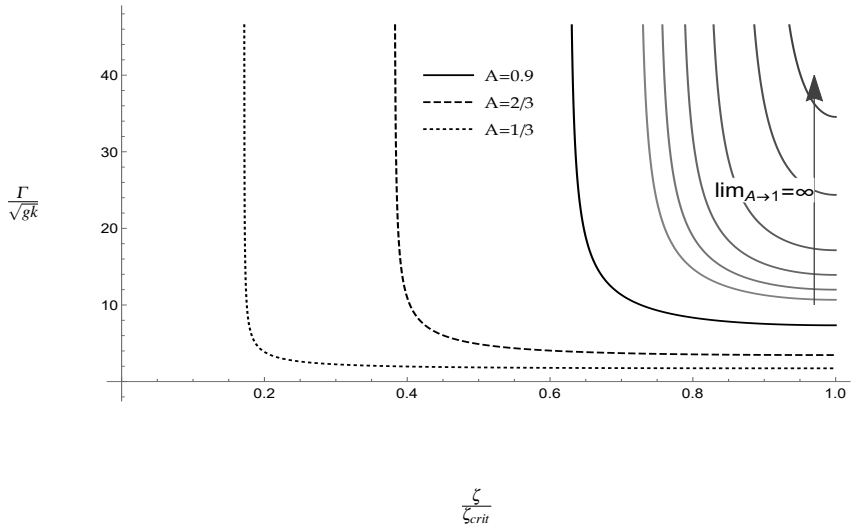

Fig. 6 The dependence of shear (Γ) scaled by growth rate ($\sqrt{gk}$, $g = Gt^a$) on the curvature (ζ). The dynamics as $A \to 1$ is unbounded for all curvatures. In the rescaling, $g = Gt^a$

5 Conclusion

By using group theoretic methods, we have explored the linear and non-linear dynamics of the large-scale structures in Rayleigh Taylor instabilities under variable acceleration. We have considered an interface with two translational symmetries under a time-varying acceleration with power-law dependence - in particular, power-

law with exponents larger than -2. By invoking the theory of group representations. we have expanded the flow fields, derived a dynamical system from the governing equations and then found asymptotic solutions for both the bubbles and spikes that emerged (Equations 12).

For the early time regime, we found that the behaviour of bubbles and spikes can be described using a linear combination of Bessel functions (Equation 26). For non-linear bubbles and spikes, however we found asymptotic solutions with power-law time dependence. For non-linear bubbles, we have observed that for small enough curvatures, the velocity is small (Figure 4). For spikes, we have observed that the velocity does fall away for sufficiently large curvatures, but is also singular at a curvature determined by the Atwood number (Figure 5). We linked this unexpected and unusual behaviour to the interfacial shearing. For non-linear bubbles, the interfacial shear mediates the decrease in velocity that occurs at large curvatures. For the non-linear spikes, the interfacial shear induces the velocity bounding at large curvatures, but it also grows with the singular velocity that appears at sufficiently small curvatures.

We found that the shear dominates the acceleration induced dynamics in bubbles and spikes of sufficient curvature, meaning that the velocity is dependent on the interfacial shearing. The problem of Rayleigh Taylor instability therefore exhibits multi-scale dynamics and has a one-parameter family of solutions.

To conclude, we have studied the problem of Rayleigh-Taylor instability in time-varying acceleration using group theoretic methods. We have found the interface dynamics to directly depend on the interfacial shearing and revealed the multi-scale dynamics of late-time Rayleigh-Taylor nature. Our analysis has achieved excellent agreement with available observations, and gives new theoretical benchmarks for future analysis, experiments and simulations.

References

1. SI Abarzhi, Katsunobu Nishihara, and R Rosner. Multiscale character of the nonlinear coherent dynamics in the rayleigh-taylor instability. *Physical Review E*, 73(3):036310, 2006.
2. Snezhana I. Abarzhi. Review of nonlinear dynamics of the unstable fluid interface: conservation laws and group theory. *Physica Scripta*, T132:014012, dec 2008.
3. U. Alon, J. Hecht, D. Ofer, and D. Shvarts. Power laws and similarity of rayleigh-taylor and richtmyer-meshkov mixing fronts at all density ratios. *Phys. Rev. Lett.*, 74:534–537, Jan 1995.
4. David Arnett and Roger A. Chevalier. Supernovae and Nucleosynthesis: An Investigation of the History of Matter, from the Big Bang to the Present. *Physics Today*, 49(10):68,70, 1996.
5. Stephen E. Bodner, Denis G. Colombant, John H. Gardner, Robert H. Lehmberg, Stephen P. Obenschain, Lee. Phillips, Andrew J. Schmitt, John D. Sethian, Robert L. McCrory, Wolf. Seka, et al. Direct-drive laser fusion: Status and prospects. *Physics of Plasmas*, 5(5):1901–1918, 1998.
6. JP. Choi and VWS. Chan. Predicting and adapting satellite channels with weather-induced impairments. *IEEE Transactions on Aerospace and Electronic Systems*, 38(3):779–790, 2002.

7. R. M. Davies and Geoffrey Ingram Taylor. The mechanics of large bubbles rising through extended liquids and through liquids in tubes. *Proceedings of the Royal Society of London. Series A. Mathematical and Physical Sciences*, 200(1062):375–390, 1950.
8. PR Garabedian. On steady-state bubbles generated by taylor instability. *Proceedings of the Royal Society of London. Series A. Mathematical and Physical Sciences*, 241(1226):423–431, 1957.
9. Abbas Ghasemizad, Hanif Zarringhalam, and Leila Gholamzadeh. The investigation of Rayleigh-Taylor instability growth rate in inertial confinement fusion. *J. Plasma Fusion Res*, 8:1234–1238, 2009.
10. Desmond L. Hill, Aklant K. Bhowmick, Dan V. Ilyin, and Snezhana I. Abarzhi. Group theory analysis of early-time scale-dependent dynamics of the rayleigh-taylor instability with time varying acceleration. *Phys. Rev. Fluids*, 4:063905, Jun 2019.
11. Ivan P. Kaminow, Chris R. Doerr, Corrado. Dragone, Tom. Koch, Uzi. Koren, Adel AM. Saleh, Alan J. Kirby, CM. Ozveren, B. Schofield, and Robert E. Thomas. A wideband all-optical WDM network. *IEEE Journal on Selected Areas in Communications*, 14(5):780–799, 1996.
12. Rayleigh Lord. Investigation of the character of the equilibrium of an incompressible heavy fluid of variable density. *Scientific papers*, pages 200–207, 1900.
13. B. Luk'yanchuk, N. Bityurin, S. Anisimov, and D. Bäuerle. The role of excited species in UV-laser materials ablation. *Applied Physics A*, 57(4):367–374, Oct 1993.
14. Grétar Tryggvason. Numerical simulations of the rayleigh-taylor instability. *Journal of Computational Physics*, 75(2):253 – 282, 1988.